Supporting Information for "State-dependent effects of natural forcing on global and regional climate variability"

Beatrice Ellerhoff[1,2,3], Moritz J. Kirschner[1], Elisa Ziegler[1,2,3], Max D. Holloway[4], Louise Sime[5], Kira Rehfeld[1,2,3]

[1]Institute of Environmental Physics, Heidelberg, Germany

[2]Department of Physics and Department of Geoscience, Tübingen University, Tübingen, Germany

[3]Geo- und Umweltforschungszentrum, Tübingen University, Tübingen, Germany

[4]Scottish Association for Marine Science, Oban, United Kingdom

[5]British Antarctic Survey, Cambridge, United Kingdom

Contents of this file

1. Figures S1 to S11
2. Tables S1 and S2

Additional Supporting Information (Files uploaded separately)

1. Captions for Datasets S1

Introduction This supporting material provides additional information on boundary conditions, surface climate, and spectral properties of the HadCM3 simulation. We show

the power spectra of all simulated and reconstructed time series, used for variance ratio estimates. The separately uploaded dataset S1 contains detailed information about the considered paleoclimate records from Rehfeld, Münch, Ho, and Laepple (2018), Rayner et al. (2003), and the PAGES2k-Consortium (2017). We provide a supporting analysis on the contribution of sea ice dynamics to variability using the two-dimensional TransEBM model (Ziegler & Rehfeld, 2021).

Data Set S1. Key specification of proxy records used to estimate local temperature variance ratios. The records were collected from Rehfeld et al. (2018), Rayner et al. (2003) and the PAGES2k-Consortium (2017). The first six columns denote the reconstruction name, assigned ID, location (Latitude, Longitude, Elevation), archive type, and proxy used. The last column denotes the climate state ("LGM" or "PI") for which the proxy reconstruction was considered. Surface temperature observations were taken from the location closest to the proxy location and specified by "HadISST@...".

References

Berger, A. L. (1978). Long-term variations of daily insolation and Quaternary climatic changes. *Journal of Atmospheric Sciences*, *35*(12), 2361–2367. doi: 10.1175/1520-0469(1978)035⟨2362:ltvodi⟩2.0.co;2

Brad Adams, J., Mann, M. E., & Ammann, C. M. (2003). Proxy evidence for an El Niño-like response to volcanic forcing. *Nature*, *426*(6964), 274–278. doi: 10.1038/nature02101

Cox, P. M. (2001). Description of the" triffid" dynamic global vegetation model. *Hadley Centre Technical Note*.

Crowley, T. J., & Unterman, M. B. (2013). Technical details concerning development of a 1200 yr proxy index for global volcanism. *Earth System Science Data*, *5*, 187-197. doi: 10.5194/essd-5-187-2013

Danabasoglu, G., Yeager, S. G., Kwon, Y.-O., Tribbia, J. J., Phillips, A. S., & Hurrell, J. W. (2012). Variability of the atlantic meridional overturning circulation in ccsm4. *Journal of climate*, *25*(15), 5153–5172.

Fredriksen, H. B., & Rypdal, M. (2017). Long-range persistence in global surface temperatures explained by linear multibox energy balance models. *Journal of Climate*, *30*, 7157-7168. doi: 10.1175/JCLI-D-16-0877.1

Huybers, P., & Curry, W. (2006). Links between annual, milankovitch and continuum temperature variability. *Nature*, *441*, 329-332. doi: 10.1038/nature04745

Lovejoy, S., & Varotsos, C. (2016). Scaling regimes and linear/nonlinear responses of last millennium climate to volcanic and solar forcings. *Earth System Dynamics*, *7*, 133-150. doi: 10.5194/esd-7-133-2016

PAGES2k-Consortium. (2017). A global multiproxy database for temperature reconstructions of the common era. *Scientific Data*, *4*, 1-33. doi: DOI:10.1038/sdata.2017.88

Rayner, N. A., Parker, D. E., Horton, E. B., Folland, C. K., Alexander, L. V., Rowell, D. P., ... Kaplan, A. (2003). Global analyses of sea surface temperature, sea ice, and night marine air temperature since the late nineteenth century. *Journal of Geophysical Research: Atmospheres*, *108*(D14). doi: https://doi.org/10.1029/2002JD002670

Rehfeld, K., Münch, T., Ho, S. L., & Laepple, T. (2018). Global patterns of declining

temperature variability from the last glacial maximum to the holocene. *Nature*, *554*, 356-359. doi: 10.1038/nature25454

Schmidt, G. A., Jungclaus, J. H., Ammann, C. M., Bard, E., Braconnot, P., Crowley, T. J., ... Vieira, L. E. A. (2012). Climate forcing reconstructions for use in pmip simulations of the last millennium (v1.1). *Geoscientific Model Development*, *5*, 185-191. doi: 10.5194/gmd-5-185-2012

Sear, C. B., Kelly, P. M., Jones, P. D., & Goodess, C. M. (1987). Global surface-temperature responses to major volcanic eruptions. *Nature*, *330*(6146), 365–367. Retrieved from `https://doi.org/10.1038/330365a0` doi: 10.1038/330365a0

Singarayer, J. S., & Valdes, P. J. (2010). High-latitude climate sensitivity to ice-sheet forcing over the last 120 kyr. *Quaternary Science Reviews*, *29*, 43-55. doi: 10.1016/j.quascirev.2009.10.011

Steinhilber, F., Beer, J., & Fröhlich, C. (2009). Total solar irradiance during the holocene. *Geophysical Research Letters*, *36*, 1-5. doi: 10.1029/2009GL040142

Wang, Y., Lean, J. L., & Jr., N. R. S. (2005). Modeling the sun's magnetic field and irradiance since 1713. *The Astrophysical Journal*, *625*, 522-538. doi: 10.1086/429689

Zhuang, K., North, G. R., & Stevens, M. J. (2017). A netcdf version of the two-dimensional energy balance model based on the full multigrid algorithm. *SoftwareX*, *6*, 198-202. doi: 10.1016/j.softx.2017.07.003

Ziegler, E., & Rehfeld, K. (2021). Transebm v. 1.0: Description, tuning, and validation of a transient model of the earth's energy balance in two dimensions. *Geoscientific Model Development*, *14*, 2843-2866. doi: 10.5194/gmd-14-2843-2021

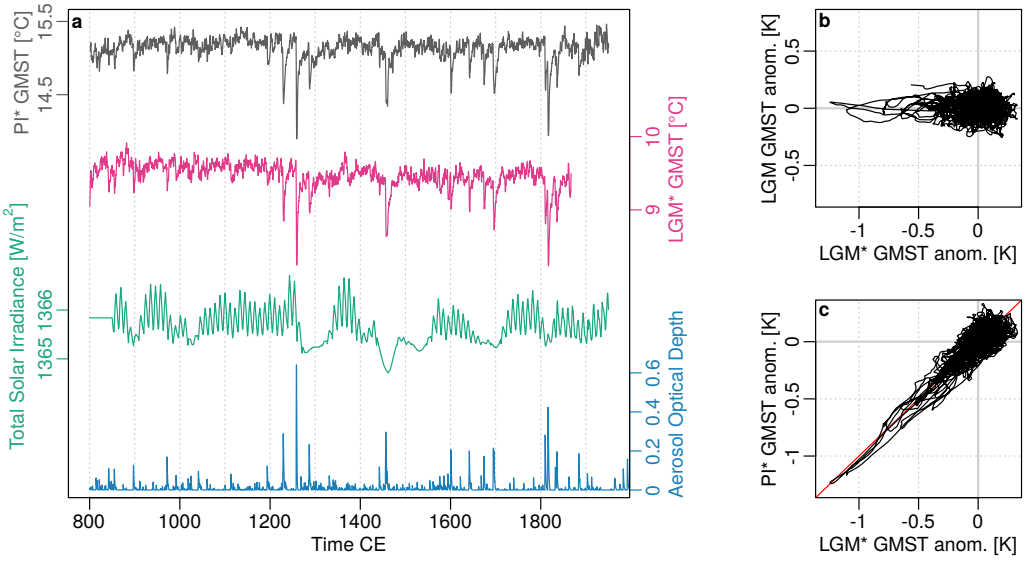

Figure S1. **a** Simulated PI* and LGM* global mean surface temperature (GMST) averaged over all runs in a state, total solar irradiance (Steinhilber et al., 2009), and aerosol optical depth (Crowley & Unterman, 2013). The solar forcing was kept constant the first 50 years due to missing reconstructions. **b** LGM over LGM* GMST anomalies from HadCM3 after linear detrending and subtracting the mean of the full time series. **c** As **b**, with PI* over LGM* GMST anomalies.

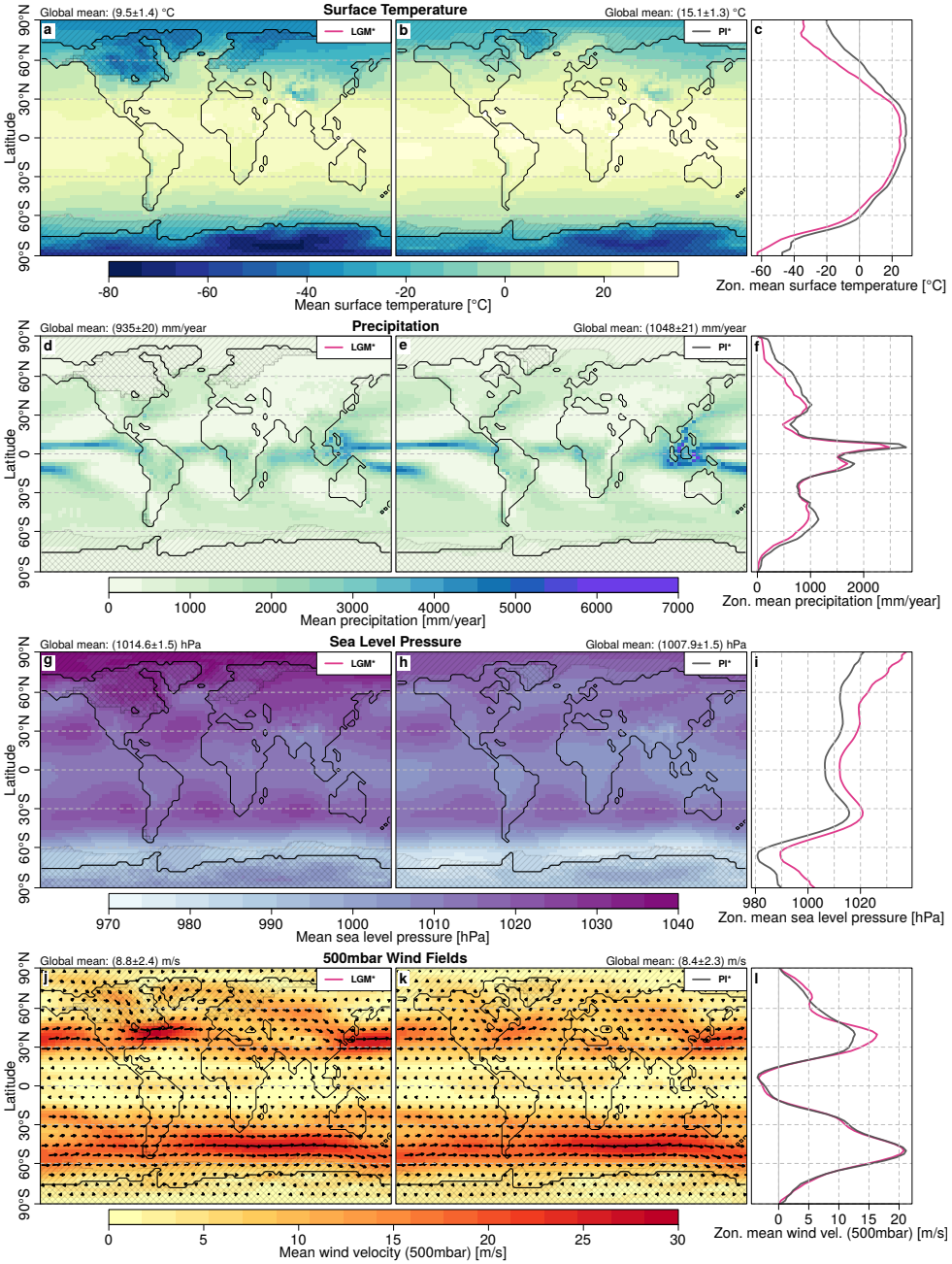

Figure S2. Surface temperature (**a-c**), precipitation rate (**d-f**), sea level pressure (**g-i**), and wind fields at 500mbar (**j-l**) as simulated by HadCM3 for the LGM* and PI*. Means over latitude intervals are displayed in the right-hand panels. Global mean values and their standard deviation are given above the maps.

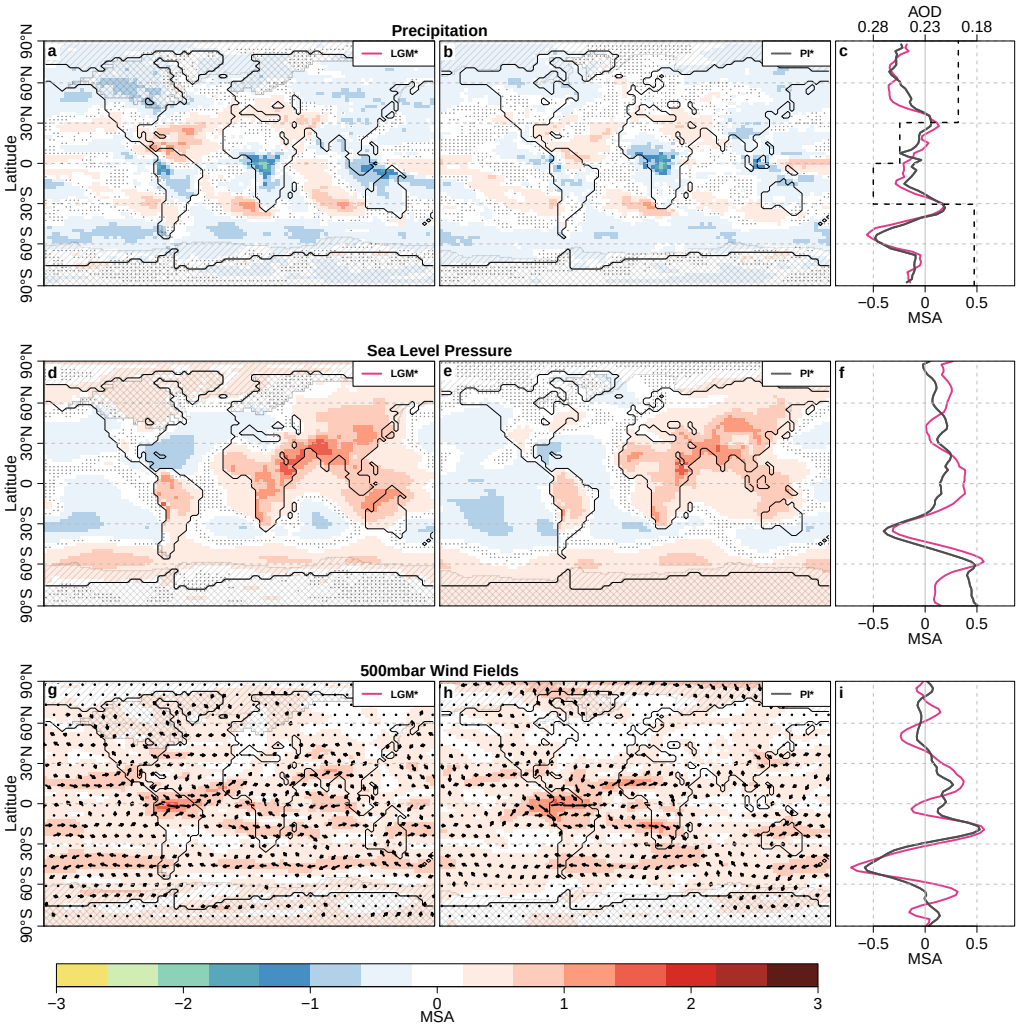

Figure S3. Mean standardized anomalies (MSA), as Figure 2 of the main manuscript, for precipitation rate (**a-c**), sea level pressure (**d-f**), and wind fields at 500mbar (**g-i**) from HadCM3. Dots indicate insignificant anomalies within the 99% quantile range of local variability. Grey shaded crosses and lines show land and sea ice, respectively. Mean anomalies over latitude intervals are displayed on the right-hand panels. The black dashed line shows the mean zonal Aerosol Optical Depth (AOD) imprint.

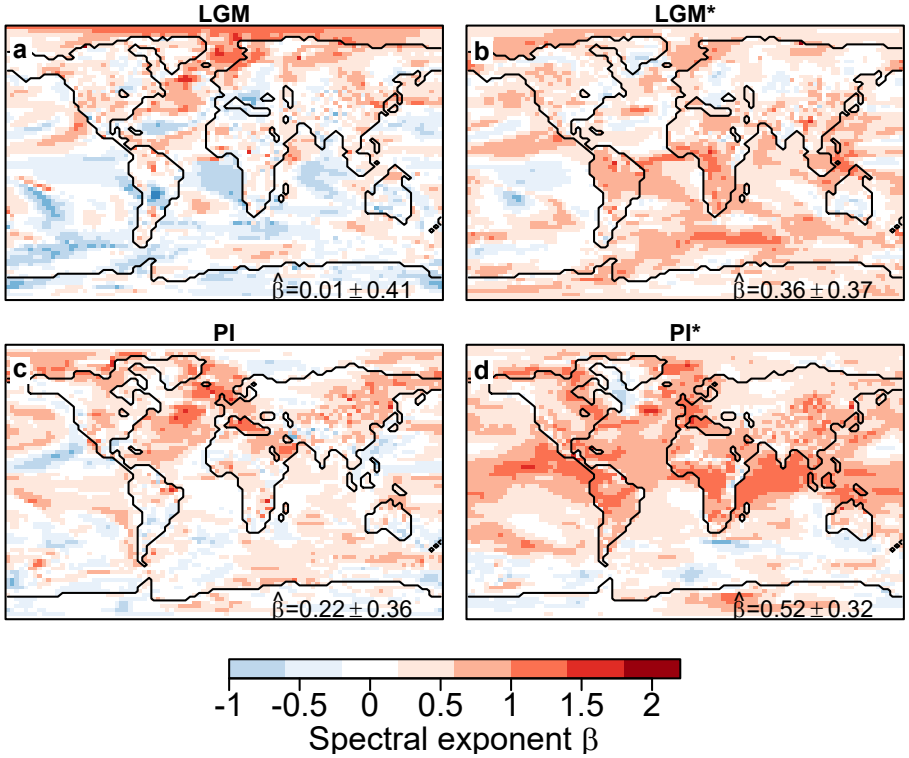

Figure S4. Scaling coefficient β of forced and unforced surface air temperature on the multidecadal-to-multicentennial scale (50-500yrs) as simulated by HadCM3 for the Last Glacial and Pre-Industrial. Surface air temperature variability was approximated by power-laws of the spectrum $S(\tau) \sim \tau^{\beta}$ with $50 \leq \tau \leq 500$ years and scaling coefficient β (Huybers & Curry, 2006; Fredriksen & Rypdal, 2017; Lovejoy & Varotsos, 2016). The area-weighted mean scaling coefficient is denoted by $\hat{\beta}$. Following Huybers and Curry (2006), we estimate β by linear regression after log-binning to prevent low-frequency biases.

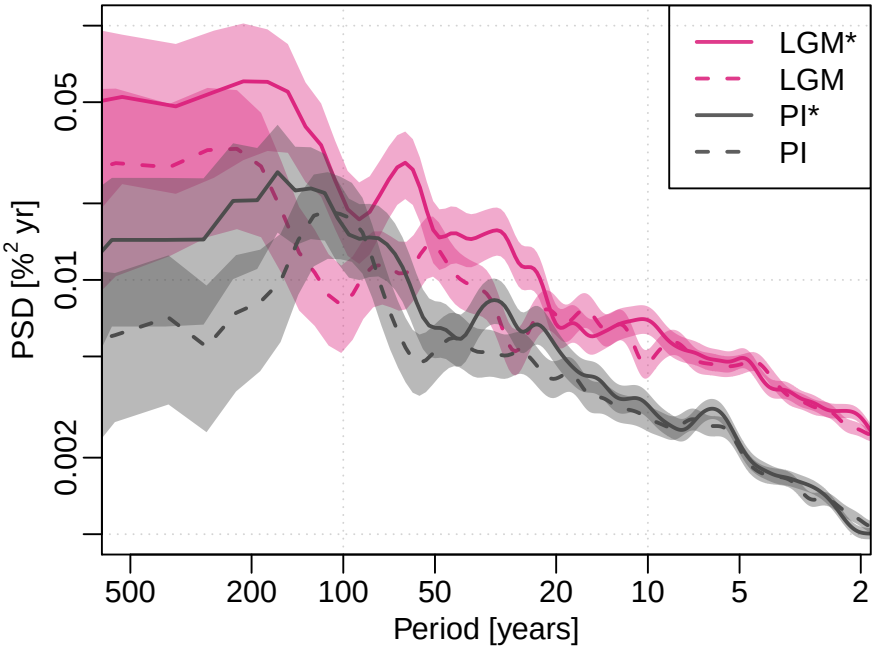

Figure S5. Power spectral density (PSD) of naturally forced and unforced global mean sea ice concentration as simulated by HadCM3 using Last Glacial and Pre-Industrial boundary conditions. The global mean sea ice concentration is defined as the percentage of the globe covered in sea ice.

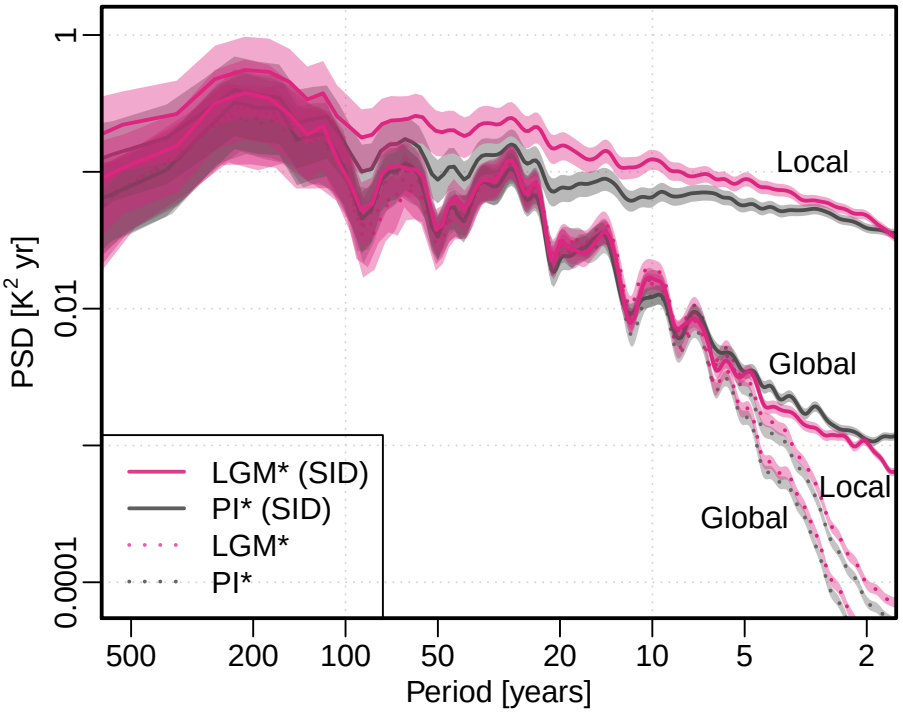

Figure S6. Global and local mean spectra of naturally forced surface air temperature as simulated by TransEBM with (solid lines) and without (dotted lines) time-varying sea ice dynamics (SID). TransEBM is a two-dimensional energy balance model with T42 resolution, as described by Ziegler and Rehfeld (2021) which draws on Zhuang et al. (2017). We run TransEBM with the same boundary conditions and time-varying forcing time series as the HadCM3 simulations, including the latitudinal-dependent volcanic forcing. Without loss of generality, we used the same constant CO2 values as in HadCM3 and neglected minor impacts from other greenhouse gases. The EBM is driven by yearly averaged solar and volcanic forcing. Dotted lines show the global and local mean spectra of the simulated temperature when sea ice extent is fixed. To mimic the sea ice dynamics in the two-dimensional model, we update the EBM's land-sea mask yearly based on the sea ice output from HadCM3 and repeat the simulations.

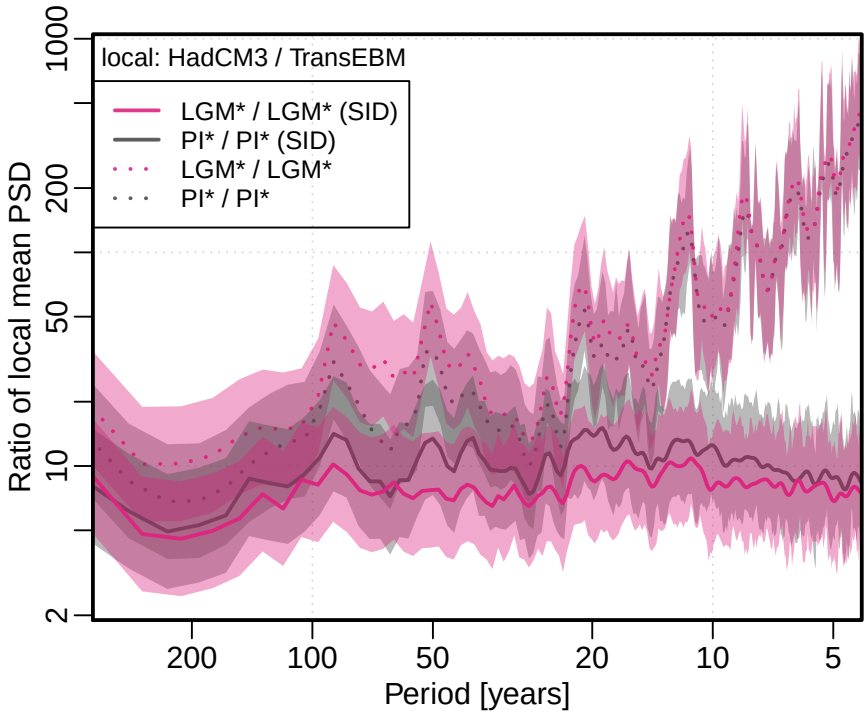

Figure S7. Ratio of HadCM3 (Figure 3) to TransEBM (Figure S6) local mean spectra (PSD) of naturally forced surface air temperature. LGM* / LGM* and PI* / PI* denote the ratios obtained from dividing the local mean spectrum of the naturally forced HadCM3 temperature by the one obtained from TransEBM with fixed sea ice. For the ratios of LGM* / LGM* (SID) and PI* / PI* (SID), time-varying sea ice dynamics in TransEBM was prescribed using the HadCM3 output. Hence, forming the ratio largely removes the linear response to naturally forcing and, for (SID), the contribution to variability from sea ice. The ratios therefore indicate the timescale-dependency of local variance simulated by HadCM3 that can be mainly attributed to internal dynamics excluding (solid lines) and including (dotted lines) sea ice dynamics. Shaded confidence intervals are computed from the F-distribution, based on the degrees of freedom of the spectral estimates.

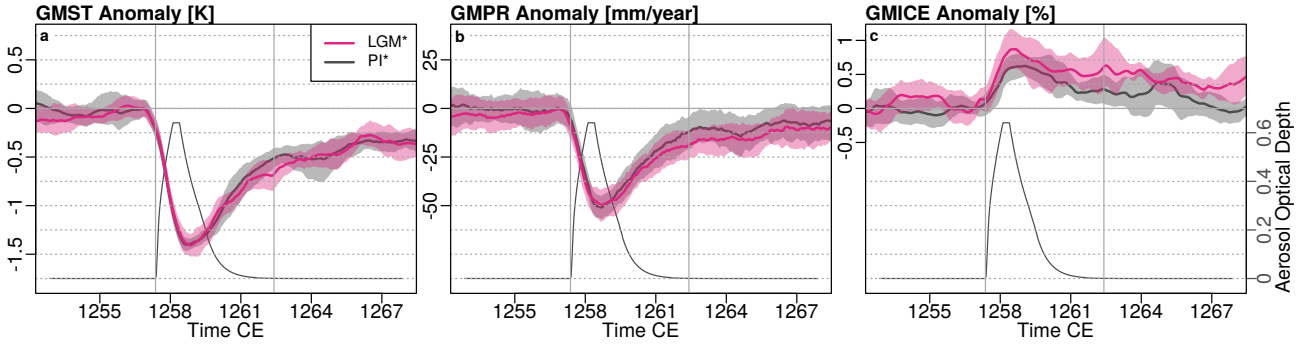

Figure S8. Superposed epoch analysis (see e.g., Sear et al. (1987); Brad Adams et al. (2003)) of globally averaged surface temperature (GMST, **a**), precipitation rate (GMPR, **b**), and sea ice concentration (GMICE, **c**) as simulated by HadCM3 using the reconstructed 1257 Samalas eruption. The lines represent the average value over all simulations in the LGM* and PI* state, and the shaded areas their respective ranges. The volcanic forcing from the Samalas eruption is shown in black. Anomalies are calculated against the three-year period before the eruption using the deseasonalized, detrended HadCM3 model output.

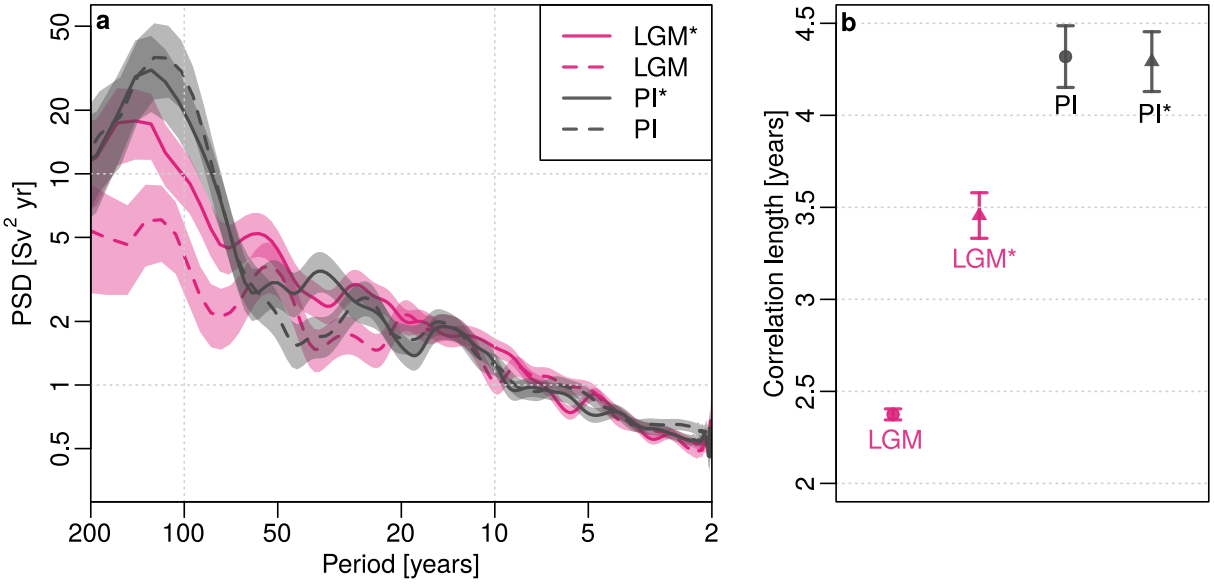

Figure S9. **a** Power spectral density (PSD) of the Atlantic Meridional Overturning Circulation (AMOC) strength from control and forced LGM and PI simulations using HadCM3. **b** Correlation length, defined as the lag at which the autocorrelation function first drops below 1/e and its standard error. Following Danabasoglu et al. (2012), we compute the AMOC strength as the maximum of the meridional ocean velocity field between 450 m and 2100 m depth and 20°N to 62.5°N at every timestep. Accordingly, the AMOC strength is given in Sv = 10^6 m^3 s^{-1}. The correlation length is an average of 3000 randomly sampled 100 year time slices of each state (1000 slices per run).

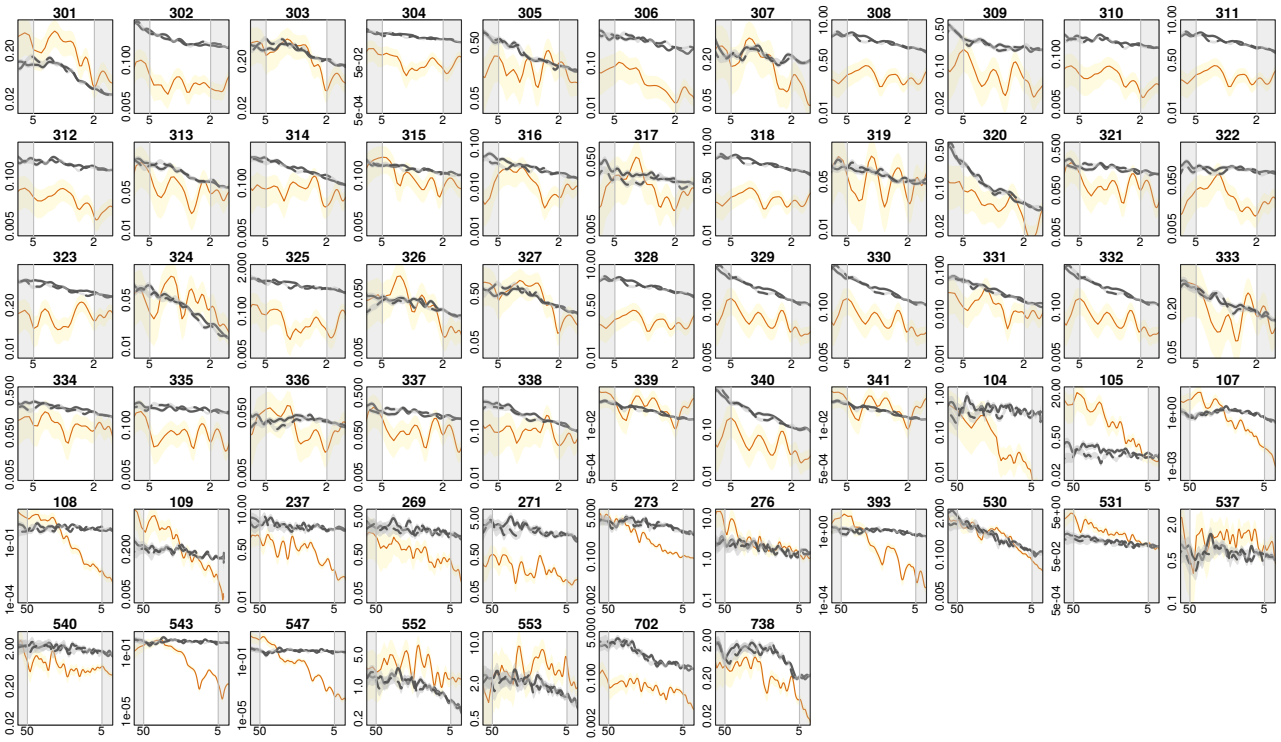

Figure S10. Temperature spectra from observations and proxy records (orange), and from HadCM3 simulations (grey) for the Pre-Industrial state, used for variance ratio estimates (Figure 4 of the main manuscript). The x-axis labels and background of each panel highlights the period (2-5 and 5-50 years) considered for timescale-dependent variance estimates. The y-axis denotes the power spectral density. Solid and dashed lines indicate forced and unforced runs. The title denotes the IDs from the separately uploaded dataset S1.

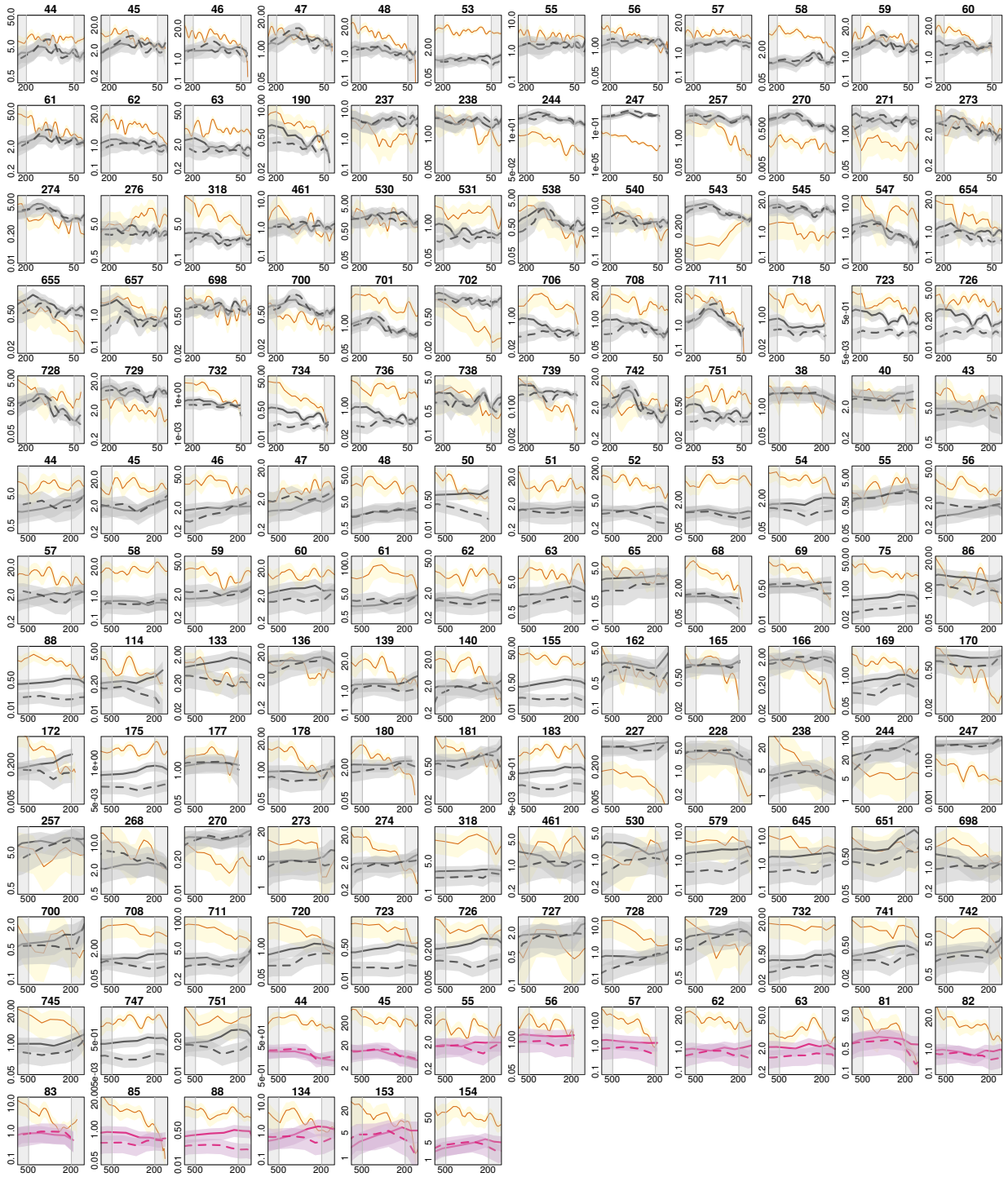

Figure S11. Same as Figure S10 but for multidecadal (50-200 years) and multicentennial (200-500 years) timescales. HadCM3 simulations under Last Glacial boundary conditions are shown in magenta.

Table S1. Boundary conditions of the HadCM3 simulation ensemble. Orbital parameters are internally calculated following (Berger, 1978) and Orography is taken from Singarayer and Valdes (2010) for 21 ka BP and 1850 CE. Greenhouse gas concentrations are taken from the protocols of the PMIP3 21ka and PI experiments (Schmidt et al., 2012). Vegetation is modeled with a 30-year timestep (Cox, 2001). Forced runs are driven by time-varying volcanic and solar (volc + sol) forcing as described in Table S2.

State	**Orography, Orb. Param.**	**CO_2, CH_4, N_2O**	**Forcing**	**#Runs**
Last Glacial Maximum (LGM)	21 ka BP	185ppm, 350ppb, 200ppb	–	3
Forced LGM (LGM*)	21 ka BP	185ppm, 350ppb, 200ppb	volc + sol	3
Pre-Industrial (PI)	1850 CE	280ppm, 650ppb, 270ppb	–	3
Forced PI (PI*)	1850 CE	280ppm, 650ppb, 270ppb	volc + sol	3

Table S2. Key specifications of the HadCM3 simulation ensemble. We provide the main references of the solar and volcanic forcing, whereby "-" indicates no forcing at all. The climate state defines the orography, orbital parameters, and greenhouse gas concentrations according to Table S1. The temporal resolution of each run is one month. The final column denotes the number of simulated years.

Name	Run ID	Climate state	Solar Forcing	Volcanic Forcing	Duration (yrs)
lgm1	xmzka	LGM	1365 W/m^2	–	1117
lgm2	xmzkd	LGM	1365 W/m^2	–	1066
lgm3	xmzki	LGM	1365 W/m^2	–	523
lgm4	xmzke	LGM*	Steinhilber et al. (2009); Wang, Lean, and Jr. (2005)	Crowley and Unterman (2013)	1064
lgm5	xmzkg	LGM*	Steinhilber et al. (2009); Wang et al. (2005)	Crowley and Unterman (2013)	1058
lgm6	xmzkh	LGM*	Steinhilber et al. (2009); Wang et al. (2005)	Crowley and Unterman (2013)	931
pi1	xnage	PI	1365 W/m^2	–	1055
pi2	xnagh	PI	1365 W/m^2	–	560
pi3	xnagb	PI	1365 W/m^2	–	1124
pi4	xnagd	PI*	Steinhilber et al. (2009); Wang et al. (2005)	Crowley and Unterman (2013)	1062
pi5	xnagf	PI*	Steinhilber et al. (2009); Wang et al. (2005)	Crowley and Unterman (2013)	1095
pi6	xnagg	PI*	Steinhilber et al. (2009); Wang et al. (2005)	Crowley and Unterman (2013)	1150